Journal of Colloid and Interface Science 698 (2025) 137928

Contents lists available at ScienceDirect

Journal of Colloid And Interface Science

journal homepage: www.elsevier.com/locate/jcis

Regular Article

Curvature-dependent adsorption of surfactants in water nanodroplets and nanobubbles

Fabio Staniscia *, Matej Kanduč

Department of Theoretical Physics, Jožef Stefan Institute, Jamova 39, Ljubljana, SI-1000, Slovenia

GRAPHICAL ABSTRACT

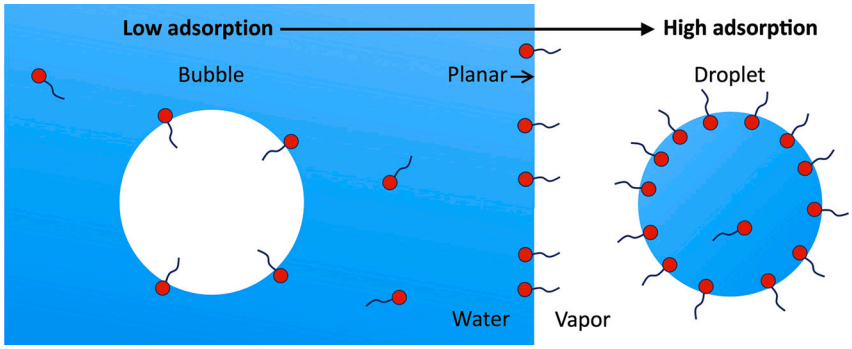

ARTICLE INFO

Dataset link: 10.5281/zenodo.15202309

Keywords:
Droplets
Bubbles
Surfactants
Adsorption
Molecular dynamics simulation

ABSTRACT

Hypothesis: Surfactants, molecules that readily adsorb to liquid interfaces and reduce surface tension, are paramount to numerous natural and technological processes: from cloud formation and climate modeling to the stability and reactivity of nanodroplets and nanobubbles. While surfactant adsorption at planar interfaces has been well-studied, their behavior at curved interfaces remains much less understood. Since curvature modifies interfacial thermodynamic properties, we hypothesize that it will also affect surfactant adsorption.
Simulations: To test this hypothesis, we perform molecular dynamics simulations of short-chain surfactants at water–vapor interfaces with varying curvature, examining droplets, bubbles, and planar interfaces.
Findings: The outcomes reveal a systematic dependence of adsorption on curvature, which is enhanced at droplet interfaces and reduced at bubble interfaces, with the effect becoming more pronounced for surfactants with longer alkyl tails. We attribute this curvature-dependent behavior to two key mechanisms: Laplace pressure and curvature-dependent surface tension. The breakdown of these contributions allows us to obtain a quantitative understanding and to predict the influence of curvature on adsorption.

1. Introduction

The interface where water meets air is known for attracting a variety of small and large molecules. Surfactants, in particular, hold a special place owing to their amphiphilic structure, which gives them unique capabilities to orient and self-assemble along this boundary. By reducing surface tension, surfactants facilitate the stabilization of foams and emulsions in natural, environmental, and industrial processes [1–4].

The air–water interface is one of the most thoroughly studied interfaces and serves as a foundational model for exploring the complex

* Corresponding author.
E-mail address: fabio.staniscia@ijs.si (F. Staniscia).

https://doi.org/10.1016/j.jcis.2025.137928
Received 22 October 2024; Received in revised form 13 May 2025; Accepted 18 May 2025
Available online 26 May 2025

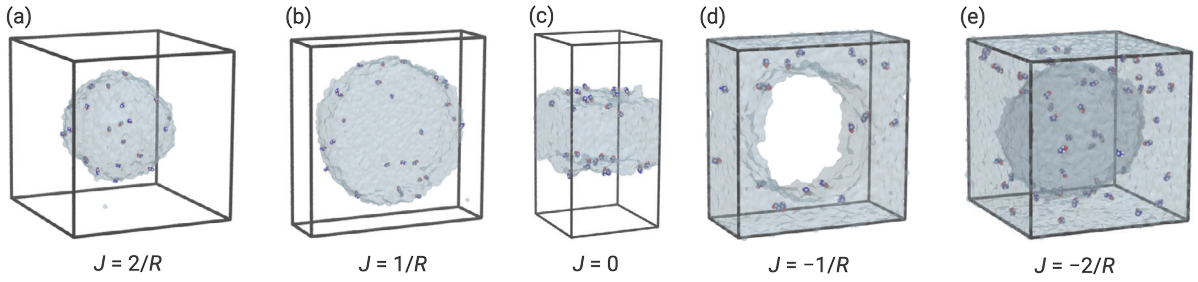

Fig. 1. Simulation snapshots representing five principal geometries in our study: (a) spherical droplet, (b) cylindrical droplet, (c) slab, (d) cylindrical bubble, and (e) spherical bubble. Surfactants (in this case propanol, C3) are shown in a united-atom representation, with alkyl groups in blue, oxygen in red, and hydrogen in white, while water is represented as a semi-transparent smoothed density isosurface.

behaviors of these molecules, providing key insights into natural phenomena and engineered applications [2,5]. Yet, despite extensive research on surfactants, the behavior of these molecules at curved water interfaces, such as those found in nanodroplets and nanobubbles, remains a largely underexplored aspect of the field.

The curvature effects are of particular significance for atmospheric aerosols—the most abundant type of aqueous nanodroplets on the planet—which play a critical role in Earth's climate and atmospheric chemistry. Aerosols contain a substantial organic component, originating from both natural sources (e.g., vegetation, sea spray) and human activities (e.g., urban pollution) [6–8]. Amphiphilic molecules in aerosols (alcohols, amines, acids, etc.) reduce the surface tension and the nucleation barrier of these particles to form cloud droplets, thereby participating in climate regulation [9–12]. However, the precise mechanisms of these processes, particularly the role of surfactants, remain a major uncertainty in current climate models [13]. A deeper understanding of how surfactants behave and adsorb within nanodroplets can help refine climate model predictions.

Moreover, organic molecules on aqueous nanodroplets alter their chemical reactivity and reaction pathways, which differ from those in bulk water [14,15]. Certain chemical reactions are accelerated by several orders of magnitude at water interfaces [16], predominantly because of much higher reactant concentrations at these locations. The discovery of this 'on-water catalysis' has spurred extensive research into its impact on atmospheric, environmental, biological, and prebiotic chemistries, simultaneously opening new avenues for the development of green synthetic processes [17].

Conversely, nanobubbles represent scenarios of negative curvatures relative to droplets. The stability of nanobubbles is a complex and debated topic, crucial in various applications where their presence is either beneficial or detrimental [18–20]. The role of surfactants on nanobubble dynamics and stability has been widely investigated [18,21]. By adsorbing to nanobubble interfaces, surfactants can lower surface tension, hinder gas exchange between the bubble and the liquid, and relax the pinning of the three-phase contact line at the substrate [21]. Notably, nanobubbles can be successfully stabilized by insoluble surfactants, which adsorb at their interface—a principle exploited in stable nano- and microbubbles used as ultrasound contrast agents [22,23]. Surface nanobubbles can form during photochemical or electrochemical processes when high concentrations of gases produced at electrodes lead to their nucleation [18,24]. Surfactants can reduce the nucleation barrier, thus facilitating the growth of these nanobubbles while simultaneously hindering the diffusion of gas molecules into the surrounding solution [25].

A major challenge in understanding these phenomena is that the properties of water interfaces in ultrafine droplets and bubbles are not well understood, largely because of the inherent difficulties of performing experiments and characterizing surfaces at such small scales [26]. In this realm, molecular modeling offers valuable insights. In the past decade, several computer simulation studies have focused on the adsorption of molecules in nanodroplets [27–30], although only a handful of them recognized that the curvature of the water interface may impact its affinity to surfactants [28,29]. Simulations [31] and experiments [32] have indicated that curvature can also influence adsorption onto solid nanoparticles. Despite its fundamental importance, this phenomenon has not been thoroughly investigated in a systematic study.

To address this knowledge gap, we conduct a molecular dynamics (MD) simulation study of the adsorption behavior of a homologous series of short-chain linear alcohols in water nanodroplets and nanobubbles of various sizes. This straightforward and insightful model system allows us to identify the underlying physics of curvature effects, governed by Laplace pressure and curvature-dependent surface tension. Additionally, we develop a simple theory, which provides explanation and predictive insights for longer-chained amphiphilic molecules.

2. Methods

2.1. Simulation model

To investigate how the curvature of water interfaces affects the adsorption of small nonionic amphiphilic molecules, we developed a molecular model in different setups for MD simulations. We construct water droplets and vapor bubbles in spherical and cylindrical morphologies, as well as a water slab. Snapshots of all five geometries are shown in Fig. 1.

Notably, the vapor bubbles in our simulations are stabilized by the negative pressure in the surrounding water phase. The pressure difference across the water–vapor interface corresponds to the Laplace pressure, just as in the case of gas bubbles in water at atmospheric pressure. Thus, this setup serves as an effective model for gas bubbles under atmospheric conditions. Furthermore, the cylindrical morphology for droplets and bubbles, albeit less realistic, is often used in theoretical and simulation studies because of practical reasons, including simplified implementation, ease of analysis, and reduced computational cost. In our work, the cylindrical morphology provides a means for testing the broader applicability of the concept of curvature.

In these aqueous systems, we investigate the behavior of surfactants by considering six linear alcohols with increasing alkyl chain lengths: methanol (C1), ethanol (C2), propanol (C3), pentanol (C5), octanol (C8), and dodecanol (C12).

2.2. Simulation details

MD simulations were conducted using the GROMACS 2019 and 2023 packages [33], employing the SPC/E water model [34] and the united-atom GROMOS force field [35] for surfactants. The structures and topology files for surfactants were obtained from the ATB repository [36]. Electrostatic interactions were treated using the particle–mesh Ewald method [37,38] with a real-space cutoff of 0.9 nm. Lennard-Jones interactions were also truncated at 0.9 nm to ensure consistency with our previous study [39]. A time step of 2 fs was used for integration. The system temperature was maintained at 300 K using the velocity-rescaling thermostat [40] with a time constant of 0.1 ps. Equilibration

was achieved by allowing the system to evolve for 10 ns under these conditions prior to data sampling.

The water slab simulations were based on our previous work [39], where a 5-nm-thick water slab was placed in a rectangular simulation box measuring 5 nm × 5 nm × 10 nm. Cylindrical droplets were simulated in rectangular boxes with a fixed axial length of 5 nm, and lateral dimensions varying from 10 to 18 nm, depending on the droplet radius. Spherical droplets were simulated in cubic boxes with sizes ranging from 12 to 16 nm. In the case of cylindrical bubbles, the axial length was kept fixed at 5 nm, while lateral dimensions ranged from 8 to 11 nm. Spherical bubbles were simulated in cubic boxes ranging from 9 to 13 nm in size.

All simulations were performed in the constant-volume (NVT) ensemble with periodic boundary conditions applied in all three dimensions. The number of water molecules in our simulations ranged from approximately 2,000 in the smallest droplets to 48,000 in the largest bubble simulations. The number of surfactant molecules varied depending on the species. In most cases, it remained below 70 in droplet and slab simulations, and reached up to 270 in bubble simulations. The simulation input files are available in an open-access repository (see Data availability statement).

For each surfactant type and concentration, we typically performed four independent 100 ns simulations for droplets. For the largest droplets of each surfactant, only three realizations were conducted, as the larger number of molecules requires fewer realizations for adequate sampling. However, in the case of pentanol, we combined sixteen droplet simulations at two different concentrations to ensure reliable statistics. Simulations of spherical bubbles were limited to three 40 ns replicas, as the larger surrounding water phase provided sufficient sampling within a shorter timescale. Only a single simulation was sufficient for octanol and dodecanol, as we sampled only their interfacial structures.

3. Results and discussion

3.1. Simulations: adsorption

The central descriptor in our analysis is the *mean curvature* of an interface, J, defined as

$$J = \frac{1}{R_1} + \frac{1}{R_2}, \tag{1}$$

where R_1 and R_2 represent the principal radii of curvature. In particular, for a spherical droplet with radius R (Fig. 1a), the curvature is convex and defined as $J = 2/R$ (with $R_1 = R_2 = R$), whereas for cylindrical droplets (Fig. 1b), the curvature is $J = 1/R$ (with $R_1 = R$ and $R_2 \to \infty$). As the radius of curvature increases (decreasing J), we approach the limiting case of a planar (i.e., flat) water–vapor interface, characterized by zero curvature ($J = 0$), modeled as a water slab (Fig. 1c). Moving on to bubble geometries, which have concave interfaces, the curvature becomes negative, with $J = -1/R$ for cylindrical (Fig. 1d) and $J = -2/R$ for spherical bubbles (Fig. 1e).

The exchange time of surfactants between the water–vapor interface and the bulk increases exponentially with alkyl chain length, roughly tripling with each additional CH_2 group, as demonstrated in Section S1 in the Supplementary Material. The exchange times range from about 0.4 ns for methanol (C1) to approximately 40 ns for pentanol (C5). For octanol (C8) and dodecanol (C12), the exchange times are estimated to reach ~1 μs and ~100 μs, respectively—well beyond the timescales accessible in unbiased simulations for achieving adequate sampling. C8 and C12 remain largely adsorbed at the interface throughout the simulation. Therefore, our analysis for these two surfactants is limited to their structural properties at the interface, which we discuss in the next subsection. We note that free energy methods, such as umbrella sampling or thermodynamic integration, could be employed to compute adsorption free energies for these longer-chain surfactants [27,41,42]. However, such an approach lies outside the scope of the present study, which utilizes unbiased simulations.

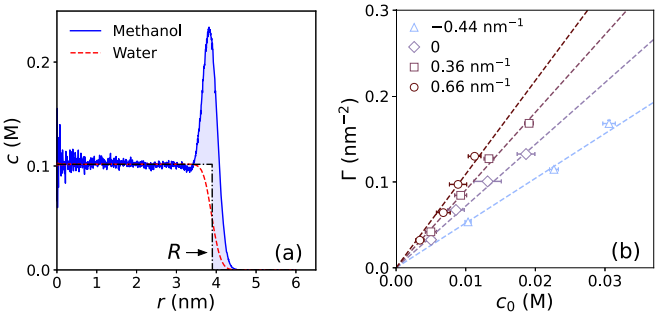

Fig. 2. (a) Radial density profiles of methanol (solid blue curve; scale on the left) and water (dashed red curve; arbitrary units) for a cylindrical droplet with a radius of 3.9 nm. The dash-dotted black line represents an effective water density profile modeled as a step function, switching from its bulk value to zero at the position of the Gibbs dividing surface, which defines the effective droplet radius R. The shaded area between the surfactant density profile and the step function corresponds to the surface excess Γ, defined via Eq. (2). (b) Adsorption isotherms showing surface excess versus bulk propanol concentration for different curvatures J. The lines are the fits of Eq. (4).

In Fig. 2a, we show typical radial density profiles for water and surfactant, using the case of methanol (C1) in a cylindrical droplet. The methanol profile shows a uniform bulk value (c_0) inside the droplet, followed by a pronounced peak at the interface, and then decays to virtually zero in the vapor phase outside the droplet.

We quantify the amount of surfactant adsorbed at the interface by the standard surface excess, Γ, defined as the surfactant surplus across the effective water–vapor interface, located at a distance R from the center of symmetry of the droplet, bubble, or slab. This center corresponds to a point for spherical geometries, a line for cylindrical ones, and a plane for slab systems. Specifically, we calculate Γ as

$$\Gamma = \int_0^\infty c(r') \left(\frac{r'}{R}\right)^n \mathrm{d}r' - \frac{c_0 R}{n+1}, \tag{2}$$

for droplets and

$$\Gamma = \lim_{r\to\infty} \left[\int_0^r c(r') \left(\frac{r'}{R}\right)^n \mathrm{d}r' - \frac{c_0 \left(r^{n+1} - R^{n+1}\right)}{(n+1)\, R^n} \right], \tag{3}$$

for bubbles, where r is the distance from the center of symmetry of the system. Here, the exponent takes values of $n = 0$ for the slab, $n = 1$ for the cylindrical, and $n = 2$ for the spherical morphology. The effective radius of the water–vapor interface, R, corresponds to the Gibbs dividing surface, where the surface excess of water is zero.

We focus our analysis to sufficiently low concentrations of surfactants, where their adsorption is linearly proportional to the bulk concentration c_0, as described by Henry's law,

$$\Gamma = K\, c_0, \tag{4}$$

where K stands for the *adsorption coefficient*. Examining the low-concentration regime allows us to isolate and investigate the interactions between the surfactant molecules and the water interface without the nonlinear complexities introduced at high concentrations, such as cooperative adsorption and surface saturation. Moreover, low surfactant concentrations are relevant for a wide range of biological and environmental systems, where amphiphilic molecules often appear as trace impurities—for example, residual contaminants in water [43,44] or naturally occurring species in atmospheric aerosols [6].

The adsorption isotherm, describing the relationship between surface excess (Γ) and bulk concentration (c_0), is shown in Fig. 2b for propanol (C3) at four different interface curvatures. The simulation data

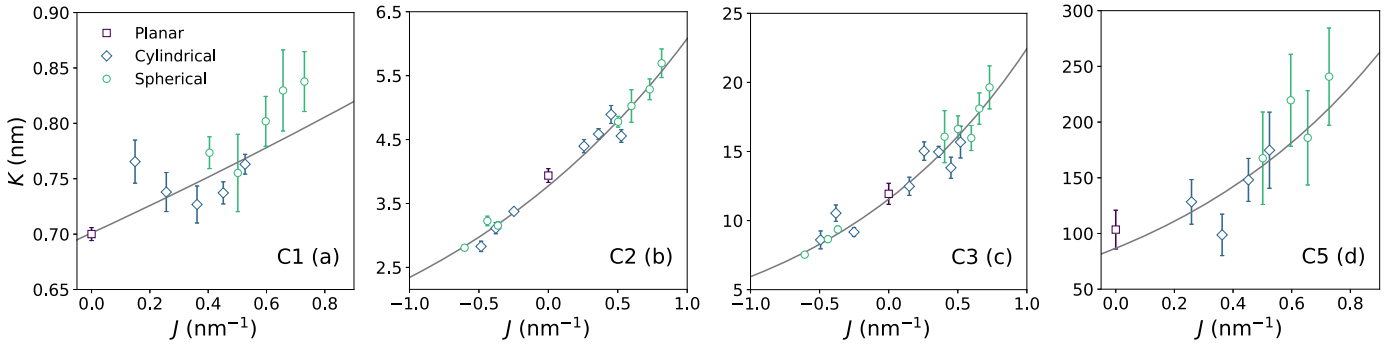

Fig. 3. Adsorption coefficient versus curvature resulting from different geometries (indicated by different symbols) for (a) methanol, (b) ethanol, (c) propanol, and (d) pentanol. Each data point is obtained by fitting Eq. (4) to the corresponding adsorption isotherm, as shown in Supplementary Material, Fig. S2. Solid curves are the fits of Eq. (9), with ξ and $K(0)$ as fitting parameters.

are fitted to Henry's law, Eq. (4), confirming the linear regime. Importantly, these outcomes clearly demonstrate that adsorption at a specific concentration is influenced by the curvature of the water–vapor interface. The adsorption isotherms for all surfactants are provided in the Supplementary Material, Fig. S2, confirming that the simulated concentrations lie below the threshold where deviations from linearity occur. These deviations arise from interactions between adsorbed surfactants, and the crossover concentrations—beyond which nonlinear behavior becomes significant—range from approximately 10 M for C1 to 10 mM for C5 (see Section S2 in the Supplementary Material).

To delve deeper into the observed curvature-dependent adsorption, we present in Fig. 3 the evaluated adsorption coefficients, K, as a function of curvature, incorporating data from all five morphologies (shown in Fig. 1) for surfactants with chain lengths up to C5. The bubble morphologies were simulated only for C2 and C3 to demonstrate the continued decreasing trend of adsorption with negative curvature values ($J < 0$). The adsorption coefficients are predominantly governed by the hydrophobic effect of the nonpolar alkyl chain, leading to an approximately exponential increase with its length [45,39].

Importantly, the results for both spherical and cylindrical morphologies align well when expressed in terms of curvature, indicating that the mean curvature J, as defined by Eq. (1), serves as a robust and effective descriptor for this phenomenon. The plots reveal a clear trend: adsorption coefficients increase with increasing curvature. These findings indicate that convexly curved water–vapor interfaces have a higher affinity to surfactants compared to planar interfaces, and even more so than concave interfaces, characterized by negative curvature.

3.2. Simulations: organization of surfactants

The above outcomes prompt the questions of why curvature influences adsorption, and what are the underlying mechanisms behind this phenomenon.

It is important to emphasize that in the linear adsorption regime, interactions between surfactant molecules are negligible. These interactions become relevant only at higher concentrations, where nonlinear adsorption behavior sets in—an effect that can be understood from the principles of the virial expansion [39]. Therefore, the dependence on curvature of the adsorption coefficient K must arise solely from how an individual surfactant interacts with the water–vapor interface. To begin addressing this question, we examine whether curvature alters the structural organization of adsorbed surfactants—such as their orientation and positioning—which could, in turn, influence their adsorption behavior.

The orientation of surfactants is a commonly considered structural parameter of adsorbed monolayers [46–48], which has been closely linked to their adsorption affinity [49–52]. We describe the orientation by the tilt angle, θ, of the tail vector with respect to the interface normal, as illustrated in Fig. 4a. The cosine of the tilt against different curvatures is plotted in Fig. 4b. As seen, the impact of curvature on molecular orientation is minor in most cases, with methanol showing a bit more noticeable effect. Thus, we conclude that the influence of interfacial curvature on molecular orientation is generally negligible for explaining variations in adsorption with curvature.

It is also insightful to examine how the tilt depends on the chain length. This relationship is plotted in Fig. 4c for a droplet of a radius of 3.35 nm. We observe a nearly linear dependence, described by

$$\langle \cos\theta \rangle \simeq \cos\theta_0 - \alpha\, n_C \tag{5}$$

where n_C denotes the number of carbon atoms in the alkyl chain. The fit yields $\cos\theta_0 = 0.79(2)$ and $\alpha = 0.039(4)$. This result indicates that shorter surfactants tend to align more perpendicularly to the interface, while those with longer chains exhibit a progressively greater tilt toward the interface. This behavior arises from a balance of competing interactions: the hydrophilic hydroxyl group favors immersion in the aqueous phase, promoting a perpendicular alignment, while the hydrophobic tail prefers to remain at the interface, thereby promoting a more tilted configuration [53]. Additionally, molecular bending may contribute to the observed tilt at higher chain lengths, as indicated by the estimated persistence length of approximately 0.77 nm (see Supplementary Material, Section S3).

The other structural parameter that we analyze is the positioning of the adsorbed surfactants relative to the water–vapor interface. We define Δr as the distance between the surfactant density peak and the Gibbs dividing surface of the water–vapor interface (located at a distance R). In Fig. 4d, we plot Δr against curvature for all surfactants. A positive Δr indicates that the surfactant's center of mass is located in the vapor phase, while a negative value suggests it resides in the water phase. From the data, we infer that the position of the surfactants relative to the interface is generally not strongly influenced by curvature. However, a slight effect is observed for bubbles and a more pronounced increase for C5 and C12 at a planar interface. In the vast majority of cases, we find $|\Delta r| \lesssim 0.05$ nm, indicating that the centers of surfactants remain close to the Gibbs dividing surface. This suggests that approximately half of the adsorbed molecule is in contact with water, while the other half with the vapor phase. In essence, adsorption leads to the dehydration of roughly one-half of the surfactant molecule.

3.3. Theoretical adsorption model

The analysis above (Fig. 4) has shown that the geometrical arrangement of adsorbed surfactants is not significantly affected by interface curvature. This implies that the adsorption affinity is affected predominantly by solvation thermodynamics. The two primary thermodynamic factors that distinguish curved water–vapor interfaces from planar ones are curvature-dependent surface tension and Laplace pressure, both of which will be explored in the following. Here, it is important to note

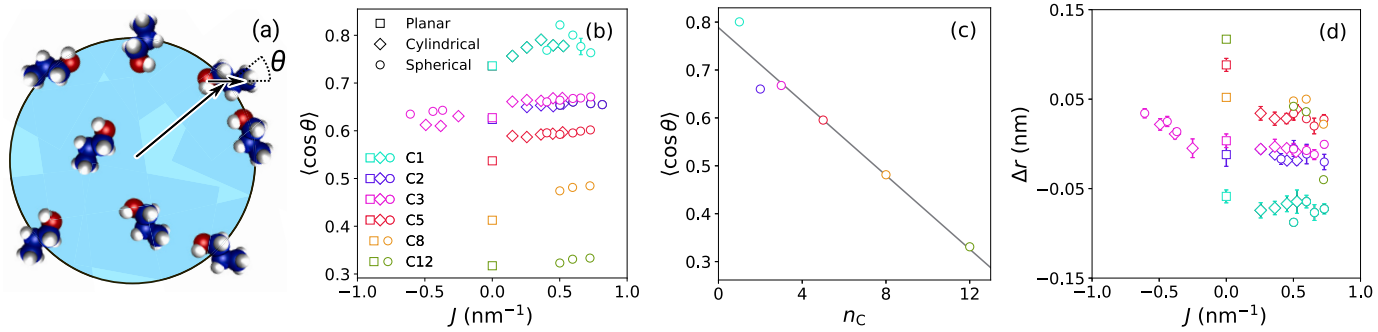

Fig. 4. (a) Schematic illustration of surfactant organization in a droplet. The blue area is bulk water, with the black line denoting the water–vapor interface. The tilt angle θ is defined between the surfactant axis and the normal of the water–vapor interface. (b) Mean tilt of surfactants at the interface against curvature. (c) Mean tilt as a function chain length on a spherical droplet of radius $R = 3.35$ nm ($J = 0.60$ nm^{-1}). The solid line denotes the fit of Eq. (5). (d) Distance between the surfactant adsorption peak and the effective water–vapor interface (R) for different curvatures; legend as in panel (b).

that while droplet or bubble size—and thus curvature—affects oscillation modes and capillary waves, these have been shown to have minimal impact on solvation thermodynamics at the liquid–vapor interface [54].

It has been known since Tolman [55], that the surface tension of a highly curved liquid interface differs from that of a planar interface. In the first-order expansion in J, the water–vapor surface tension can be expressed as

$$\gamma(J) \simeq \gamma_0 (1 - \delta_T J), \tag{6}$$

where γ_0 is the surface tension of the planar interface, and δ_T is the Tolman length. Numerous computer simulations have indicated that δ_T is on the order of angstroms for water [56–59], thus justifying the first-order expansion in Eq. (6), since $R \gg |\delta_T|$ is basically always the case.

Surface tension is a key factor in the free energy of adsorption. When a molecule adsorbs to a water–vapor interface, it eliminates the area of the interface equal to its bare cross-sectional area, A_c [39]. The free energy associated with this elimination is $-\gamma(J)A_c$, making it curvature-dependent.

The other mechanism involves the Laplace pressure across the water–vapor interface, which can be expressed as $\Delta p = \gamma_0 J$ to the first order in J. When a molecule is partially expelled from the water phase, the free energy gain equals $-\Delta p \Delta V_{mol}$, where ΔV_{mol} is the dehydrated (i.e., expelled) volume of the molecule. This effect has been recognized in studies of colloid adsorption at spherical liquid–liquid interfaces, as for instance, in Pickering emulsions [60,61]. Yet, while well understood at the colloidal scale, its impact on molecular adsorption remains largely unexplored.

We now combine these two thermodynamic factors to formulate an expression for the adsorption free energy, which represents the free energy change of transferring a surfactant from the bulk phase to the interface, viz.

$$\Delta G(J) = \Delta G_{mol} - \gamma(J) A_c - \Delta p(J) \Delta V_{mol}. \tag{7}$$

The aforementioned elimination of the water–vapor interface and the work performed by the Laplace pressure are described by the second and third terms, respectively. The first term, which is independent of curvature, is included for completeness and is associated with the molecule's dehydration and other effects not captured by the other two terms. However, since this term is independent of curvature, it is not relevant to our analysis.

The adsorption coefficient is proportional to the Boltzmann factor of the adsorption free energy, $K \propto \exp(-\Delta G / k_B T)$, where k_B is the Boltzmann constant and T the absolute temperature [39]. A comparison between the coefficients of a curved, $K(J)$, and planar interface, $K(0)$, yields

$$K(J) = K(0) \exp\left(\frac{\Delta G(0) - \Delta G(J)}{k_B T} \right). \tag{8}$$

Using the expression for the adsorption free energy, Eq. (7), in combination with the curvature-dependent surface tension, Eq. (6), leads to the following exponential dependence of the adsorption coefficient on curvature

$$K(J) = K(0) e^{\xi J}. \tag{9}$$

Here, we have introduced the *modulation radius*:

$$\xi \equiv \frac{\gamma_0}{k_B T} \Delta V_{mol} - \frac{\gamma_0 \delta_T}{k_B T} A_c, \tag{10}$$

which provides the characteristic scale at which curvature begins to considerably influence adsorption.

We begin by validating the theoretical model by fitting the parameter ξ in Eq. (9) to the simulation data in Fig. 3. The resulting fits are represented by solid lines. The exponential nature of the relationship is particularly evident for the C2 and C3 surfactants, owing to a broader range of curvatures analyzed. The fitted values of the modulation radius, ξ, are presented in Fig. 5, plotted against alkyl chain length. As seen, ξ is on the order of a nanometer and increases with chain length, indicating that surfactants with longer tails are more influenced by curvature.

To further test the robustness of the simulation results, we performed additional simulations for water–propanol systems using two alternative setups. In the first one, we increased the cutoff length to 1.4 nm while keeping the same SPC/E–GROMOS combination. In the second one, we employed TIP4P/2005 water [62] together with the CHARMM36 force field [63] for propanol, using a cutoff length of 1.2 nm. Details and the analysis of these simulations are provided in Section S4 of the Supplementary Material. These alternative setups yielded somewhat different values for the adsorption coefficient, reflecting its exponential sensitivity to the adsorption free energy. However, the extracted values of the modulation radius ξ from these two test cases—plotted in Fig. 5 alongside the main results—are in close agreement with those from our primary simulations. The fact that ξ remains considerably more consistent across different simulation conditions than the adsorption coefficient itself is due to its linear dependence on molecular properties, as suggested by Eq. (10).

In the remainder of our study, we aim to theoretically predict the modulation radius using Eq. (10) and compare these predictions to the values obtained from simulations. To do so, we have to determine the necessary parameters: the surface tension (γ_0) and Tolman length (δ_T), associated with the used SPC/E water model, as well as the surfactant-specific quantities, namely the cross-sectional area (A_c) and the dehydrated volume (ΔV_{mol}).

The two water-related parameters were extracted from three 100 ns simulations of cylindrical droplets with four different radii, performed in the absence of surfactants. During these simulations, we sampled the diagonal components of the pressure tensor (P_{xx}, P_{yy}, P_{zz}) and used

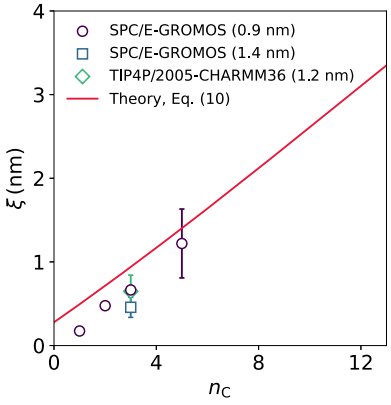

Fig. 5. Modulation radius as a function of chain length, fitted from MD simulations results (data points) and estimated from Eq. (10) (solid line).

them to define an *apparent surface tension*, which we introduce as a convenient quantity for analyzing curvature effects:

$$\tilde{\gamma} = \frac{L_x L_y}{\pi R}\left(\frac{P_{xx}+P_{yy}}{2} - P_{zz}\right). \tag{11}$$

The apparent surface tension is related to the actual surface tension of the planar interface, γ_0, and the Tolman length, δ_T, via

$$\tilde{\gamma}(J) \equiv \gamma_0 (1 - 2\delta_T J). \tag{12}$$

Note that the factor of 2 in the second term differs from the corresponding relation in Eq. (6), reflecting the specific definition used here for the apparent surface tension. The derivation of this expression is provided in Section S5 of the Supplementary Material.

By combining simulation results from the cylindrical and planar geometries, we established the relationship between $\tilde{\gamma}$ and J, as shown in Fig. S4 in the Supplementary Material. Fitting Eq. (12) to the simulation data yields a planar surface tension of $\gamma_0 \simeq 54.80(2)$ mN/m, which is in very good agreement with a previous study that used the same cutoff and water model [64]. The fit also provides a Tolman length of $\delta_T \simeq -0.078(3)$ nm, which is in reasonable agreement with the previous study ($\delta_T \simeq -0.05$ nm [64]), given its sensitivity to the fitting procedure and system size. A negative Tolman length implies that surface tension increases with decreasing droplet size and decreases with decreasing bubble size; see Eq. (6).

The sign and magnitude of the Tolman length for water are broadly consistent with values reported in most previous studies [65–68], although the literature shows considerable variation, including some disagreement on the sign [56,69]. These discrepancies likely stem from differences in water models, cutoff schemes, system sizes, and analysis methods, and they represent an ongoing open question in the field. Additional simulations using a longer cutoff length for SPC/E water and using TIP4P/2005 water, presented in Section S5 of the Supplementary Material, further support the consistency of our results. Although the value of δ_T was extracted from cylindrical droplet simulations, it should be applicable to spherical geometries as well [70], since differences between spherical and cylindrical geometry would only arise in higher-order terms of the curvature expansion in Eq. (6).

To determine the surfactant-specific quantities, we opt for a simple continuum description for surfactants. While ΔV_{mol} could in principle be calculated using idealized molecular geometries [71,72], we aim for an even simpler and more pragmatic approach. As concluded from the data in Fig. 4d, roughly half of the molecule becomes dehydrated upon adsorption from the bulk phase. We thus estimate the dehydrated volume as $\Delta V_{mol} \approx v_{mol}/2$, where v_{mol} is the entire volume of the molecule. This level of approximation is appropriate given the inherent limitations of continuum-based descriptions at the molecular scale.

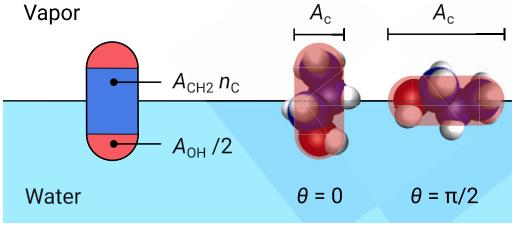

Fig. 6. Simplified model of a surfactant at the water–vapor interface, represented as a cylinder with hemispherical caps at both ends. Its lateral area is estimated from the area of the alkyl chain, while the area of the caps corresponds to the area of the OH group. The cross-sectional area A_c can be easily calculated for the two limiting cases of perpendicular ($\theta = 0$) and parallel ($\theta = \pi/2$) orientations.

The volume is best described by the partial molecular volume, which corresponds to the change in the volume of an aqueous system upon insertion of a molecule at constant pressure and temperature, defined as $v_{mol} = (\partial V/\partial N)_{p,T}$. As described in the Supplementary Material, Section S6, we evaluate these volumes by simulating different surfactant concentrations and analyzing the resulting increase in the simulation box volume. We find that molecular volumes scale very well with chain length, following the relationship

$$v_{mol} \simeq v_{OH} + v_{CH2}\, n_C, \tag{13}$$

where fitting the data yields $v_{OH} \simeq 0.028$ nm^3 and $v_{CH2} \simeq 0.025$ nm^3. These parameters can be interpreted as the contributions of the OH and CH_2 groups to the total molecular volume, respectively.

Subsequently, to assess the effective cross-sectional area of surfactants, A_c, the final parameter needed in Eq. (10), we first calculate the total molecular surface area of the molecule, A_{mol}, from which we infer about A_c. The molecular surface area A_{mol} is calculated using the standard method for determining the solvent-accessible surface area [73] but with a zero probe radius. The use of a zero probe radius is needed because the eliminated area of the water–vapor interface, A_c, corresponds to the bare cross-section of the molecule. The calculated values of A_{mol} are plotted in Fig. S6 (Supplementary Material, Section S7) against the chain length, n_C. Again, a clear linear relationship emerges, described by $A_{mol} = A_{OH} + A_{CH2}\, n_C$, where A_{OH} represents the contribution from the OH group, and A_{CH2} is the contribution from one CH_2 group in the alkyl chain. Fitting the data yields $A_{OH} \simeq 0.37$ nm^2 and $A_{CH2} \simeq 0.23$ nm^2.

To estimate A_c from A_{mol}, we approximate the surfactant as a cylinder capped with hemispheres, as illustrated in Fig. 6. We account for different tilts with the help of two limiting orientations: In the first one, the surfactant is aligned perpendicular to the interface ($\theta = 0$), and the cross-sectional area is equivalent to the circular cross-section of the cylinder or the spherical cap, given by $A_{OH}/4$. The factor $1/4$ stems from the ratio between a sphere's area and its cross-section area. In the second limit, where the surfactant lies parallel to the interface ($\theta = \pi/2$), the cross-sectional area increases by the cylindrical portion, resulting in $A_{OH}/4 + A_{CH2} n_C/\pi$, where the factor $1/\pi$ stems from the ratio between the cylinder's lateral area and its cross-section area. For an arbitrary tilt angle θ, calculating the exact cross-sectional area is mathematically involved. Therefore, we use a practical approach by interpolating between these two limiting cases, with $\sin\theta$ serving as the interpolating factor, leading to

$$A_c \simeq \frac{1}{4} A_{OH} + \frac{1}{\pi} A_{CH2}\, n_C \sin\theta. \tag{14}$$

This relation reveals that adsorption depends not only on the number of carbon atoms, but also on the surfactants' molecular orientation.

Although a persistence length of 0.77 nm (as estimated in Supplementary Material, section S3) implies that longer surfactant molecules may bend, this bending does not significantly affect the geometrical parameters used in Eq. (10). The molecular volume is largely insensitive to bending, and the cross-sectional area is only weakly affected, since

Table 1
Parameters extracted from MD simulations.

Parameter	Symbol	Value
Surface tension of a planar interface	γ_0	54.80(2) mN/m
Tolman length	δ_T	−0.078(3) nm
Tilt parameter, Eq. (5)	$\cos\theta_0$	0.79(2)
Tilt parameter, Eq. (5)	α	0.039(4)
Molecular volume of OH group, Eq. (13)	v_{OH}	0.028 nm^3
Molecular volume of CH_2 group, Eq. (13)	v_{CH2}	0.025 nm^3
Molecular area of OH group, Eq. (14)	A_{OH}	0.37 nm^2
Molecular area of CH_2 group, Eq. (14)	A_{CH2}	0.23 nm^2

shorter surfactants exhibit minimal bending, while longer chains tend to lie nearly parallel to the interface (Fig. 4c), reducing the impact of bending on their projected area.

We now finally use the calculated values for $\Delta V_{mol} = v_{mol}/2$ from Eq. (13), A_c from Eq. (14), and $\sin\theta \to (1 - \langle\cos\theta\rangle^2)^{1/2}$ from Eq. (5), along with the values of δ_T and γ_0, to predict the modulation radius using Eq. (10). The used parameters are listed in Table 1, and the prediction is shown as a solid line in Fig. 5. The comparison with simulation-determined values of ξ is semi-quantitative. Given the underlying approximations in the continuum model applied to the molecular scale, this is very good agreement, which effectively demonstrates the mechanisms through which curvature influences adsorption.

Our theoretical model also enables predictions of curvature effects for longer-chain surfactants (beyond C5), the dynamics of which are not fully captured by our simulations. As seen, the modulation radius ξ increases almost linearly with chain length. Slight deviations from linearity occur because of the $\sin\theta$ factor. Essentially, longer surfactants are influenced already by weaker curvatures. Surfactants with chain lengths around 12 are particularly common in technological applications. For dodecanol (C12), the value of ξ reaches approximately 3 nm. To illustrate the impact of curvature, we consider a case where the adsorption coefficient changes by 10%. Based on Eq. (9), this corresponds to a droplet or bubble radius of $R = 2\xi/\ln(1.1) \approx 60$ nm. This length scale highlights the importance of amphiphilic molecules in aerosols. Recent studies have shown that ultrafine aerosol particles below 50 nm in size, which are prevalent in the troposphere, can serve as significant cloud condensation nuclei, promoting the formation of cloud droplets under supersaturation conditions [10,11].

It is insightful to decompose the modulation radius in Eq. (10) into the contributions stemming from the volume (Laplace pressure) and cross-section area (Tolman length) terms. For longer chains, $n_C \gg 1$, the ratio of the area to volume terms is approximately $2|\delta_T|A_{CH2}/\pi v_{CH2} \simeq 0.5$. This indicates that both contributions are nearly comparable in size and that both should be considered in adsorption processes.

3.4. Extended discussion

While alkyl tail length is a key factor influencing adsorption and surface tension, other molecular features, such as the nature and orientation of the head group [41], also play important roles. In addition, structural branching in the hydrophobic tail has been shown to significantly affect interfacial properties [74]. These observations illustrate the complexity of surfactant behavior at interfaces and suggest further directions to extend the model to a broader range of molecules.

Although we examined only water–vapor interfaces, the same mechanisms should apply to curved liquid–liquid interfaces, such as in oil-in-water or water-in-oil emulsions [75]. In such systems, the organization of surfactants might differ due to better solubilization of alkyl tails in the oil phase [76]. Furthermore, these principles are also partially applicable to adsorption on nanoparticles [31,32,77,78] or on carbon nanotubes [79,80], where only the area term is operative. In such cases, the molecule cannot penetrate the solid, rendering the volume term in Eq. (10) inoperative.

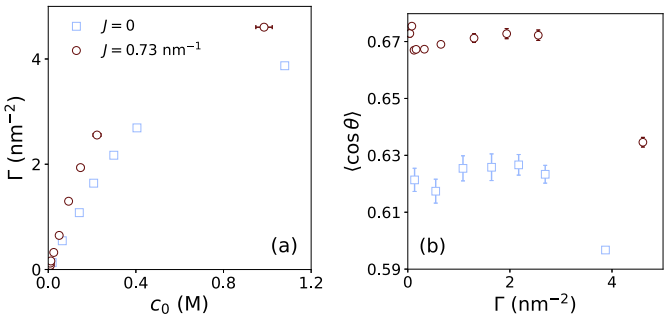

Fig. 7. (a) Adsorption isotherms for propanol (C3), shown for planar and spherical interfaces. (b) Mean tilt angle of adsorbed surfactants versus surface excess, based on the same simulations as in panel (a).

In this work, we have defined the adsorption coefficient relative to the bulk water phase. However, for volatile molecules, their concentration in the gas phase may serve as a more relevant reference. When defining the adsorption coefficient relative to the gas phase, the area term in Eq. (10) remains the same, but the volume term reverses sign. This implies that, for a given concentration of molecules in the gas phase, adsorption may be more favorable on planar water interfaces than on water droplets.

Finally, we emphasize that this study has focused on low surfactant concentrations, where Henry's law applies, which allowed us to isolate and analyze the fundamental interaction mechanisms of surfactants with the water interface. While many environmental and biological systems involve low surfactant concentrations, industrial applications such as emulsification, detergency, and enhanced oil recovery typically operate at higher concentrations. High concentrations lead to additional nonlinear phenomena, such as cooperative adsorption, surface saturation, and micelle formation, which warrant further investigation.

To assess the relevance of curvature-dependent adsorption beyond the linear regime, we examined the behavior at high concentrations. For this purpose, we conducted simulations of propanol (C3) in spherical droplets and compared the results with those previously obtained for a planar interface [39]. As shown in Fig. 7a, curvature continues to influence adsorption isotherms even at higher concentrations. Furthermore, the orientation analysis in Fig. 7b reveals that the mean tilt angle of surfactants begins to change only at high surface coverages, reflecting the onset of surfactant–surfactant interactions. These results extend the relevance of curvature and provide a solid foundation for future work exploring curvature effects in more complex, high-concentration scenarios.

4. Conclusions

In this study, we have demonstrated that the adsorption isotherms of amphiphilic molecules at water–vapor interfaces are significantly influenced by the interfacial curvature, primarily rooted in Laplace pressure and curvature-dependent surface tension. Curvature enhances adsorption in droplets and reduces it in bubbles, with the effect becoming more pronounced for surfactants with longer alkyl tails.

Despite its relevance, this phenomenon has remained largely unrecognized and unquantified, with only limited prior research on the topic [28,29] and lacking a systematic characterization or predictive theory. Our approach combines extensive MD simulations with a data analysis framework that generalizes the Gibbs dividing surface to curved interfaces, enabling precise calculations of droplet sizes and excess surfactant adsorption.

A key limitation in this field is the absence of experimental data on curvature-dependent adsorption. Future work should focus on experimental validation, either directly or through measurable consequences of curvature effects, which are manifold. For instance, smaller droplets exhibit a higher affinity for surfactant adsorption, leading to increased

surface concentrations—a factor that could play a role in observed size-dependent surfactant activity in aerosols [7] and in processes of aerosol formation and stability [10,11]. This effect should not be confused with the bulk depletion effect, which arises from the larger surface-to-volume ratio in smaller droplets [12,81]. Conversely, smaller bubbles may exhibit lower contaminant densities than larger ones, potentially affecting their stability and reactivity. Curvature-dependent adsorption also contributes to the apparent line tension of nanodroplets and nanobubbles when contaminated with surfactants [43,82]. Moreover, the adsorption affinity impacts the reaction-limited rate of surfactant exchange between the interface and the bulk phase [83]. Our results suggest that this exchange is slower in small droplets and faster in nanobubbles compared to planar interfaces, indicating a curvature-dependent dynamic equilibrium.

Lastly, while our study has focused on surfactants because of their well-characterized interfacial behavior, we believe that the principles uncovered here are broadly applicable to other hydrophobic molecules, small colloidal particles, and potentially to proteins as well.

CRediT authorship contribution statement

Fabio Staniscia: Writing – original draft, Investigation, Conceptualization. **Matej Kanduč:** Writing – review & editing, Investigation, Conceptualization, Funding acquisition.

Declaration of competing interest

The authors declare that they have no known competing financial interests or personal relationships that could have appeared to influence the work reported in this paper.

Acknowledgements

Authors acknowledge financial support from the Slovenian Research and Innovation Agency ARIS (contracts P1-0055 and J1-4382).

Appendix A. Supplementary material

Supplementary material related to this article can be found online at https://doi.org/10.1016/j.jcis.2025.137928.

Data availability

The simulation data are available at 10.5281/zenodo.15202309.

References

[1] Milton J. Rosen, Joy T. Kunjappu, Surfactants and Interfacial Phenomena, John Wiley & Sons, 2012.
[2] Robert Aveyard, Surfactants: in Solution, at Interfaces and in Colloidal Dispersions, Oxford University Press, 2019.
[3] R.J. Pugh, Foaming, foam films, antifoaming and defoaming, Adv. Colloid Interface Sci. 64 (1996) 67–142.
[4] Daniela Georgieva, Alain Cagna, Dominique Langevin, Link between surface elasticity and foam stability, Soft Matter 5 (10) (2009) 2063–2071.
[5] J. Eastoe, J.S. Dalton, Dynamic surface tension and adsorption mechanisms of surfactants at the air–water interface, Adv. Colloid Interface Sci. 85 (2–3) (2000) 103–144.
[6] Mohd Talib Latif, Peter Brimblecombe, Surfactants in atmospheric aerosols, Environ. Sci. Technol. 38 (24) (2004) 6501–6506.
[7] Ana Kroflič, Sanja Frka, Martin Simmel, Heike Wex, Irena Grgić, Size-resolved surface-active substances of atmospheric aerosol: reconsideration of the impact on cloud droplet formation, Environ. Sci. Technol. 52 (16) (Aug 2018) 9179–9187.
[8] Violaine Gérard, Barbara Noziere, Ludovic Fine, Corinne Ferronato, Dharmendra Kumar Singh, Amanda A. Frossard, Ronald C. Cohen, Eija Asmi, Heikki Lihavainen, Niku Kivekäs, Minna Aurela, David Brus, Sanja Frka, Ana Cvitešić Kušan, Concentrations and adsorption isotherms for amphiphilic aurfactants in PM1 aerosols from different regions of Europe, Environ. Sci. Technol. 53 (21) (2019) 12379–12388.
[9] John H. Seinfeld, Christopher Bretherton, Kenneth S. Carslaw, Hugh Coe, Paul J. DeMott, Edward J. Dunlea, Graham Feingold, Steven Ghan, Alex B. Guenther, Ralph Kahn, Ian Kraucunas, Sonia M. Kreidenweis, Mario J. Molina, Athanasios Nenes, Joyce E. Penner, Kimberly A. Prather, V. Ramanathan, Venkatachalam Ramaswamy, Philip J. Rasch, A.R. Ravishankara, et al., Improving our fundamental understanding of the role of aerosol-cloud interactions in the climate system, Proc. Natl. Acad. Sci. 113 (21) (2016) 5781–5790.
[10] Jiwen Fan, Daniel Rosenfeld, Yuwei Zhang, Scott E. Giangrande, Zhanqing Li, Luiz A.T. Machado, Scot T. Martin, Yan Yang, Jian Wang, Paulo Artaxo, Henrique M.J. Barbosa, Ramon C. Braga, Jennifer M. Comstock, Zhe Feng, Wenhua Gao, Helber B. Gomes, Fan Mei, Christopher Pöhlker, Mira L. Pöhlker, Ulrich Pöschl, Rodrigo A.F. de Souza, Substantial convection and precipitation enhancements by ultrafine aerosol particles, Science 359 (6374) (2018) 411–418.
[11] Christina J. Williamson, Agnieszka Kupc, Duncan Axisa, Kelsey R. Bilsback, ThaoPaul Bui, Pedro Campuzano-Jost, Maximilian Dollner, Karl D. Froyd, Anna L. Hodshire, Jose L. Jimenez, John K. Kodros, Gan Luo, Daniel M. Murphy, Benjamin A. Nault, Eric A. Ray, Bernadett Weinzierl, James C. Wilson, Fangqun Yu, Pengfei Yu, Jeffrey R. Pierce, Charles A. Brock, A large source of cloud condensation nuclei from new particle formation in the tropics, Nature 574 (7778) (2019) 399–403.
[12] Bryan R. Bzdek, Jonathan P. Reid, Jussi Malila, Nønne L. Prisle, The surface tension of surfactant-containing, finite volume droplets, Proc. Natl. Acad. Sci. 117 (15) (2020) 8335–8343.
[13] Wei-Kuo Tao, Jen-Ping Chen, Zhanqing Li, Chien Wang, Chidong Zhang, Impact of aerosols on convective clouds and precipitation, Rev. Geophys. 50 (2) (2012).
[14] D.J. Donaldson, Veronica Vaida, The influence of organic films at the air-aqueous boundary on atmospheric processes, Chem. Rev. 106 (4) (2006) 1445–1461.
[15] D.J. Donaldson, Kalliat T. Valsaraj, Adsorption and reaction of trace gas-phase organic compounds on atmospheric water film surfaces: a critical review, Environ. Sci. Technol. 44 (3) (2010) 865–873.
[16] Kevin R. Wilson, Alexander M. Prophet, Grazia Rovelli, Megan D. Willis, Rebecca J. Rapf, Michael I. Jacobs, A kinetic description of how interfaces accelerate reactions in micro-compartments, Chem. Sci. 11 (32) (2020) 8533–8545.
[17] Manuel F. Ruiz-Lopez, Joseph S. Francisco, Marilia T.C. Martins-Costa, Josep M. Anglada, Molecular reactions at aqueous interfaces, Nat. Rev. Chem. 4 (9) (2020) 459–475.
[18] Detlef Lohse, Xuehua Zhang, Surface nanobubbles and nanodroplets, Rev. Mod. Phys. 87 (3) (2015) 981–1035.
[19] Nikolai D. Petsev, L. Gary Leal, M. Scott Shell, Universal gas adsorption mechanism for flat nanobubble morphologies, Phys. Rev. Lett. 125 (14) (2020) 146101.
[20] Beng Hau Tan, Hongjie An, Claus-Dieter Ohl, Stability of surface and bulk nanobubbles, Curr. Opin. Colloid Interface Sci. 53 (2021) 101428.
[21] Muidh Alheshibri, Jing Qian, Marie Jehannin, Vincent SJ Craig, A history of nanobubbles, Langmuir 32 (43) (2016) 11086–11100.
[22] E. Stride, N. Saffari, Microbubble ultrasound contrast agents: a review, Proc. Inst. Mech. Eng., H J. Eng. Med. 217 (6) (2003) 429–447.
[23] Muidh Alheshibri, Vincent SJ Craig, Armoured nanobubbles; ultrasound contrast agents under pressure, J. Colloid Interface Sci. 537 (2019) 123–131.
[24] Qianjin Chen, Hilke S. Wiedenroth, Sean R. German, Henry S. White, Electrochemical nucleation of stable N2 nanobubbles at Pt nanoelectrodes, J. Am. Chem. Soc. 137 (37) (2015) 12064–12069.
[25] Qianjin Chen, Long Luo, Hamaseh Faraji, Stephen W. Feldberg, Henry S. White, Electrochemical measurements of single H2 nanobubble nucleation and stability at Pt nanoelectrodes, J. Phys. Chem. Lett. 5 (20) (2014) 3539–3544.
[26] Olle Björneholm, Martin H. Hansen, Andrew Hodgson, Li-Min Liu, David T. Limmer, Angelos Michaelides, Philipp Pedevilla, Jan Rossmeisl, Huaze Shen, Gabriele Tocci, Eric Tyrode, Marie-Madeleine Walz, Josephina Werner, Hendrik Bluhm, Water at interfaces, Chem. Rev. 116 (13) (2016) 7698–7726.
[27] Jochen S. Hub, Carl Caleman, David van der Spoel, Organic molecules on the surface of water droplets–an energetic perspective, Phys. Chem. Chem. Phys. 14 (27) (2012) 9537–9545.
[28] Minoru Sayou, Ryosuke Ishizuka, Nobuyuki Matubayasi, Energetic analysis of adsorption and absorption of small molecule to nanodroplet of water, J. Phys. Chem. B 121 (24) (Jun 2017) 5995–6001.
[29] Wentao Li, Chi Yuen Pak, Ying-Lung Steve Tse, Free energy study of H_2O, N_2O_5, SO_2, and O_3 gas sorption by water droplets/slabs, J. Chem. Phys. 148 (16) (2018) 164706.
[30] Patrick K. Wise, Lyudmila V. Slipchenko, Dor Ben-Amotz, Ion-size dependent adsorption crossover on the surface of a water droplet, J. Phys. Chem. B 127 (20) (2023) 4658–4665.
[31] Matthew R. Farrow, Philip J. Camp, Peter J. Dowding, Ken Lewtas, The effects of surface curvature on the adsorption of surfactants at the solid–liquid interface, Phys. Chem. Chem. Phys. 15 (2013) 11653–11660.
[32] Zonglin Gu, Zaixing Yang, Yu Chong, Cuicui Ge, Jeffrey K. Weber, David R. Bell, Ruhong Zhou, Surface curvature relation to protein adsorption for carbon-based nanomaterials, Sci. Rep. 5 (1) (Jun 2015) 10886.
[33] David Van Der Spoel, Erik Lindahl, Berk Hess, Gerrit Groenhof, Alan E. Mark, Herman J.C. Berendsen, GROMACS: fast, flexible, and free, J. Comput. Chem. 26 (16) (2005) 1701–1718.
[34] H.J.C. Berendsen, J.R. Grigera, T.P. Straatsma, The missing term in effective pair potentials, J. Phys. Chem. 91 (24) (Nov 1987) 6269–6271.
[35] Nathan Schmid, Andreas P. Eichenberger, Alexandra Choutko, Sereina Riniker, Moritz Winger, Alan E. Mark, Wilfred F. van Gunsteren, Definition and testing of the GROMOS force-field versions 54A7 and 54B7, Eur. Biophys. J. 40 (7) (Jul 2011) 843–856.

[36] Alpeshkumar K. Malde, Le Zuo, Matthew Breeze, Martin Stroet, David Poger, Pramod C. Nair, Chris Oostenbrink, Alan E. Mark, An automated force field topology builder (ATB) and repository: version 1.0, J. Chem. Theory Comput. 7 (12) (Dec 2011) 4026–4037.
[37] Tom Darden, Darrin York, Lee Pedersen, Particle mesh Ewald: an n log(n) method for Ewald sums in large systems, J. Chem. Phys. 98 (12) (1993) 10089–10092.
[38] Ulrich Essmann, Lalith Perera, Max L. Berkowitz, Tom Darden, Hsing Lee, Lee G. Pedersen, A smooth particle mesh Ewald method, J. Chem. Phys. 103 (19) (1995) 8577–8593.
[39] F. Staniscia, H.V. Guzman, M. Kanduč, Tuning contact angles of aqueous droplets on hydrophilic and hydrophobic surfaces by surfactants, J. Phys. Chem. B 126 (17) (2022) 3374–3384, PMID: 35468298.
[40] Giovanni Bussi, Davide Donadio, Michele Parrinello, Canonical sampling through velocity rescaling, J. Chem. Phys. 126 (1) (2007) 014101.
[41] Harry Cárdenas, M. Ariif, H. Kamrul-Bahrin, Dale Seddon, Jofry Othman, João T. Cabral, Andrés Mejía, Sara Shahruddin, Omar K. Matar, Erich A. Müller, Determining interfacial tension and critical micelle concentrations of surfactants from atomistic molecular simulations, J. Colloid Interface Sci. 674 (2024) 1071–1082.
[42] Matej Kanduč, Cosima Stubenrauch, Reinhard Miller, Emanuel Schneck, Interface adsorption versus bulk micellization of surfactants: insights from molecular simulations, J. Chem. Theory Comput. 20 (4) (2023) 1568–1578.
[43] Yuki Uematsu, Douwe Jan Bonthuis, Roland R. Netz, Impurity effects at hydrophobic surfaces, Curr. Opin. Electrochem. 13 (2019) 166–173.
[44] Xinbo Zhang, Yuanying Yang, Huu Hao Ngo, Wenshan Guo, Haitao Wen, Xiao Wang, Jianqing Zhang, Tianwei Long, A critical review on challenges and trend of ultrapure water production process, Sci. Total Environ. 785 (2021) 147254.
[45] Himanshu Singh, Sumit Sharma, Hydration of linear alkanes is governed by the small length-scale hydrophobic effect, J. Chem. Theory Comput. 18 (6) (2022) 3805–3813.
[46] H. Hsiung, G.R. Meredith, H. Vanherzeele, R. Popovitz-Biro, E. Shavit, M. Lahav, Ordering of two nitroaniline-terminated amphiphiles at the air—water interface studied by optical second harmonic generation and ellipsometry, Chem. Phys. Lett. 164 (5) (1989) 539–544.
[47] Patrycja Dynarowicz, Distribution and the energetics of orientation of molecules adsorbed at the water/air interface, Colloids Surf. 59 (1991) 371–376.
[48] Victor Ekholm, Carl Caleman, Jochen S. Hub, Malin Wohlert, Propensity, free energy contributions and conformation of primary n-alcohols at a water surface, Phys. Chem. Chem. Phys. 23 (2021) 18823–18829.
[49] V.B. Fainerman, R. Miller, R. Wüstneck, A.V. Makievski, Adsorption isotherm and surface tension equation for a surfactant with changing partial molar area. 1. Ideal surface layer, J. Phys. Chem. 100 (18) (Jan 1996) 7669–7675.
[50] Francesca Ravera, Libero Liggieri, Reinhard Miller, Molecular orientation as a controlling process in adsorption dynamics, Colloids Surf. A, Physicochem. Eng. Asp. 175 (1) (2000) 51–60.
[51] V.B. Fainerman, R. Miller, E.V. Aksenenko, Adsorption behavior of oxyethylated alcohols at the solution/air interface, Langmuir 16 (9) (May 2000) 4196–4201.
[52] Valentin B. Fainerman, Volodymyr I. Kovalchuk, Eugene V. Aksenenko, Francesca Ravera, Libero Liggieri, Giuseppe Loglio, Alexander V. Makievski, Emanuel Schneck, Reinhard Miller, Thermodynamics, kinetics and dilational visco-elasticity of adsorbed cneom layers at the aqueous solution/air interface, Colloids and Interfaces 5 (1) (2021).
[53] Liu Shi, Naga Rajesh Tummala, Alberto Striolo, $C_{12}E_6$ and SDS surfactants simulated at the vacuum- water interface, Langmuir 26 (8) (2010) 5462–5474.
[54] Kaustubh Rane, Nico F.A. van der Vegt, Understanding the influence of capillary waves on solvation at the liquid-vapor interface, J. Chem. Phys. 144 (11) (2016).
[55] R.C. Tolman, The effect of droplet size on surface tension, J. Chem. Phys. 17 (3) (1949) 333–337.
[56] Felix Sedlmeier, Roland R. Netz, The spontaneous curvature of the water-hydrophobe interface, J. Chem. Phys. 137 (13) (2012) 135102.
[57] Suriyanarayanan Vaikuntanathan, Phillip L. Geissler, Putting water on a lattice: the importance of long wavelength density fluctuations in theories of hydrophobic and interfacial phenomena, Phys. Rev. Lett. 112 (Jan 2014) 020603.
[58] Mark N. Joswiak, Nathan Duff, Michael F. Doherty, Baron Peters, Size-dependent surface free energy and Tolman-corrected droplet nucleation of TIP4P/2005 water, J. Phys. Chem. Lett. 4 (24) (Dec 2013) 4267–4272.
[59] Mark N. Joswiak, Ryan Do, Michael F. Doherty, Baron Peters, Energetic and entropic components of the Tolman length for mW and TIP4P/2005 water nanodroplets, J. Chem. Phys. 145 (20) (2016) 204703.
[60] Peter A. Kralchevsky, Kuniaki Nagayama, Capillary interactions between particles bound to interfaces, liquid films and biomembranes, Adv. Colloid Interface Sci. 85 (2–3) (2000) 145–192.
[61] S. Komura, Y. Hirose, Y. Nonomura, Adsorption of colloidal particles to curved interfaces, J. Chem. Phys. 124 (24) (2006) 241104.
[62] J.L.F. Abascal, C. Vega, A general purpose model for the condensed phases of water: TIP4P/2005, J. Chem. Phys. 123 (23) (2005) 234505.
[63] J. Huang, A.D. MacKerell Jr., CHARMM36 all-atom additive protein force field: validation based on comparison to nmr data, J. Comput. Chem. 34 (25) (2013) 2135–2145.
[64] Matej Kanduč, Going beyond the standard line tension: size-dependent contact angles of water nanodroplets, J. Chem. Phys. 147 (17) (2017).
[65] Mark N. Joswiak, Nathan Duff, Michael F. Doherty, Baron Peters, Size-dependent surface free energy and Tolman-corrected droplet nucleation of tip4p/2005 water, J. Phys. Chem. Lett. 4 (24) (2013) 4267–4272.
[66] Georg Menzl, Miguel A. Gonzalez, Philipp Geiger, Frédéric Caupin, José L.F. Abascal, Chantal Valeriani, Christoph Dellago, Molecular mechanism for cavitation in water under tension, Proc. Natl. Acad. Sci. USA 113 (48) (2016) 13582–13587.
[67] Sa Hoon Min, Max L. Berkowitz, Bubbles in water under stretch-induced cavitation, J. Chem. Phys. 150 (5) (2019).
[68] Cintia P. Lamas, Carlos Vega, Eva G. Noya, Eduardo Sanz, The water cavitation line as predicted by the tip4p/2005 model, J. Chem. Phys. 158 (12) (2023).
[69] Shahrazad Malek, Peter H. Poole, Ivan Saika-Voivod, Surface tension of supercooled water nanodroplets from computer simulations, J. Chem. Phys. 150 (23) (2019).
[70] M.J.P. Nijmeijer, C. Bruin, A.B. van Woerkom, A.F. Bakker, J.M.J. van Leeuwen, Molecular dynamics of the surface tension of a drop, J. Chem. Phys. 96 (1) (1992) 565–576.
[71] Jordi Faraudo, Fernando Bresme, Stability of particles adsorbed at liquid/fluid interfaces: shape effects induced by line tension, J. Chem. Phys. 118 (14) (2003) 6518–6528.
[72] Bum Jun Park, Daeyeon Lee, Configuration of nonspherical amphiphilic particles at a fluid–fluid interface, Soft Matter 8 (29) (2012) 7690–7698.
[73] Frank Eisenhaber, Philip Lijnzaad, Patrick Argos, Chris Sander, Michael Scharf, The double cubic lattice method: efficient approaches to numerical integration of surface area and volume and to dot surface contouring of molecular assemblies, J. Comput. Chem. 16 (3) (1995) 273–284.
[74] Stephanie S. Adkins, Xi Chen, Quoc P. Nguyen, Aaron W. Sanders, Keith P. Johnston, Effect of branching on the interfacial properties of nonionic hydrocarbon surfactants at the air–water and carbon dioxide–water interfaces, J. Colloid Interface Sci. 346 (2) (2010) 455–463.
[75] Michael Gradzielski, Magali Duvail, Paula Malo de Molina, Miriam Simon, Yeshayahu Talmon, Thomas Zemb, Using microemulsions: formulation based on knowledge of their mesostructure, Chem. Rev. 121 (10) (2021) 5671–5740.
[76] Paulina Müller, Douwe Jan Bonthuis, Reinhard Miller, Emanuel Schneck, Ionic surfactants at air/water and oil/water interfaces: a comparison based on molecular dynamics simulations, J. Phys. Chem. B 125 (1) (2021) 406–415.
[77] Nicole Welsch, Yan Lu, Joachim Dzubiella, Matthias Ballauff, Adsorption of proteins to functional polymeric nanoparticles, Polymer 54 (12) (2013) 2835–2849.
[78] Elton L. Correia, Siddharth Thakur, Aanahita Ervin, Emma Shields, Sepideh Razavi, Adsorption of surfactant molecules onto the surface of colloidal particles: case of like-charged species, Colloids Surf. A, Physicochem. Eng. Asp. 676 (2023) 132142.
[79] Naga Rajesh Tummala, Alberto Striolo, Sds surfactants on carbon nanotubes: aggregate morphology, ACS Nano 3 (3) (Mar 2009) 595–602.
[80] Dongkai Shao, Kosti Tapio, Sanna Auer, J. Jussi Toppari, Vesa P. Hytönen, Markus Ahlskog, Surface characteristics control the attachment and functionality of (chimeric) avidin, Langmuir 34 (50) (2018) 15335–15342, PMID: 30398878.
[81] Alison Bain, Kunal Ghosh, Nønne L. Prisle, Bryan R. Bzdek, Surface-area-to-volume ratio determines surface tensions in microscopic, surfactant-containing droplets, ACS Cent. Sci. 9 (11) (Nov 2023) 2076–2083.
[82] Fabio Staniscia, Matej Kanduč, Apparent line tension induced by surface-active impurities, J. Chem. Phys. 157 (18) (2022) 184707.
[83] Jacob N. Israelachvili, Intermolecular and Surface Forces, Academic Press, 2011.